

## A MLPG4 (LBIE) Formulation in Elastostatics

V. Vavourakis and D. Polyzos<sup>1</sup>

**Abstract:** Very recently, Vavourakis, Sellountos and Polyzos (2006) (CMES: Computer Modeling in Engineering & Sciences, vol. 13, pp. 171–184) presented a comparison study on the accuracy provided by five different elastostatic Meshless Local Petrov-Galerkin (MLPG) type formulations, which are based on Local Boundary Integral Equation (LBIE) considerations. One of the main conclusions addressed in this paper is that the use of derivatives of the Moving Least Squares (MLS) shape functions decreases the solution accuracy of any MLPG(LBIE) formulation. In the present work a new, free of MLS-derivatives and non-singular MLPG(LBIE) method for solving elastic problems is demonstrated. This is accomplished by treating displacements and stresses as independent variables through the corresponding local integral equations and considering nodal points located only internally and externally and not on the global boundary of the analyzed elastic structure. The MLS approximation scheme for the interpolation of both displacements and stresses is exploited. The essential displacement and traction boundary conditions are easily satisfied via the corresponding displacement and stress local integral equations. Representative numerical examples that demonstrate the achieved accuracy of the proposed MLPG(LBIE) method are provided.

**Keyword:** MLPG4, LBIE, MLS, hypersingular, elastostatics

### 1 Introduction

Meshless methods have attracted considerable attention in recent years, since they seem to cir-

cumvent well known problems associated with the Finite Element Method (FEM), such as meshing, remeshing, locking and element distortion and drawbacks related to the Boundary Element Method (BEM), such as full populated matrices and requirement of the fundamental solution of the problem. Smooth Particle Hydrodynamics, Petrov-Galerkin Diffuse Element, Partition of Unity, h-p Clouds, Reproducing Kernel Particle, Point Interpolation, Element Free Galerkin, Local Boundary Integral Equation, Meshless Local Petrov-Galerkin, Boundary Node and so on, are some of the meshless methods reported so far in the literature [Atluri (2004); Liu (2003)].

Eight years ago, Atluri and co-workers proposed the Local Boundary Integral Equation (LBIE) method [Zhu, Zhang, and Atluri (1998)] and the Meshless Local Petrov-Galerkin (MLPG) method [Atluri and Zhu (1998)] as alternatives to the BEM and FEM, respectively. Both methods are characterized as “truly meshless” since no background cells are required for the numerical evaluation of the involved integrals. Properly distributed nodal points, without any connectivity requirement, covering the domain of interest as well as the surrounding global boundary are employed instead of any boundary or finite element discretization. All nodal points belong in regular sub-domains (e.g. circles for two-dimensional problems) centered at the corresponding collocation points. The fields at the local and global boundaries as well as in the interior of the sub-domains are usually approximated by the Moving Least Squares (MLS) approximation scheme. Owing to regular shapes of the sub-domains, both surface and volume integrals are easily evaluated. The local nature of the sub-domains leads to a final linear system of equations the coefficient matrix of which is sparse and not full populated.

---

<sup>1</sup> Department of Mechanical Engineering and Aeronautics, University of Patras, Patras (Greece)  
Institute of Chemical Engineering and High Temperature Process ICEHT-FORTH, Rio (Greece)

Depending on the test functions used in the weak formulation of the MLPG method, Atluri and co-workers developed six different MLPG methodologies numbered from one to six [Atluri and Shen (2002a); Atluri and Shen (2002b)]. The MLPG4 method utilizes as test functions, the fundamental solution of the differential equation (or part of the differential equation) of the problem, resulting thus to a MLPG approach that is equivalent to the LBIE method. For this reason, in the present work the LBIE method will be called from now and further MLPG(LBIE) method.

In the context of the linear elasticity, several papers dealing with MLPG(LBIE) solutions have appeared in the literature. The most representative are those of [Atluri, Sladek, Sladek, and Zhu (2000); Sladek, Sladek, and Keer (2000a); Sladek, Sladek, and Atluri (2000b); Atluri, Han, and Shen (2003); Han and Atluri (2004); Sellountos and Polyzos (2003); Sellountos and Polyzos (2005a); Sellountos and Polyzos (2005b); Sellountos, Vavourakis, and Polyzos (2005); Bodin, Ma, Xin, and Krishnaswami (2006)] while a comprehensive presentation on the application of the MLPG(LBIE) method to different types of boundary value problems one can find in the review paper of Sladek, Sladek, and Atluri (2002) and in the very recent book of Atluri (2004).

Very recently, Vavourakis, Sellountos, and Polyzos (2006) presented a comparison study on the accuracy provided by five different elastostatic MLPG(LBIE) formulations. One of the main conclusions they reached is that the use of derivatives of the MLS shape functions decreases the solution accuracy of any MLPG(LBIE) formulation. Motivated by this result, the present paper addresses a new MLPG(LBIE) method where neither MLS shape function derivatives are utilized nor singular or hypersingular integrals are involved in its final numerical implementation. Displacements and stresses are considered as independent variables and interpolated via MLS approximation functions. Although both singular and hypersingular LBIEs are employed for the representation of displacements and stresses, respectively, no singular integrals appear since all the considered nodal points are located only inter-

nally and externally and not on the global boundary of the analyzed elastic body. The essential displacement and traction boundary conditions are easily satisfied via the corresponding displacement and stress LBIEs. The paper is structured as follows. The MLS approximation scheme used for the interpolation of the unknown displacements and stresses is explained in the next section. The LBIEs for displacements and stresses as well as the numerical implementation of the proposed here MLPG(LBIE) methodology are presented in section 3. Representative numerical examples that demonstrate the accuracy of the new non-singular and MLS derivatives-free MLPG(LBIE) method are provided in section 4. Finally, in section 5 some conclusions, comments and remarks are drawn.

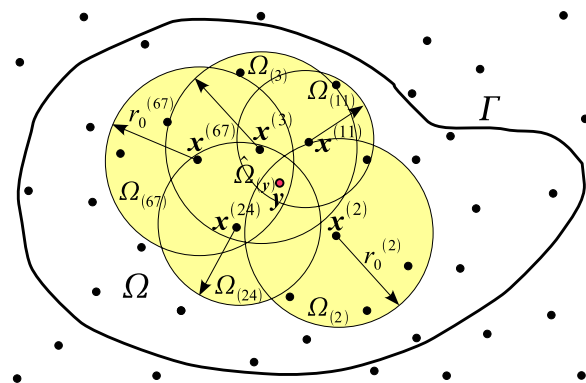


Figure 1: The circular support domains  $\Omega_{(j)}$  and the non-circular domain of definition  $\hat{\Omega}_y$  used for the approximation of the field at point  $y$

## 2 Moving Least Squares approximation scheme

Consider an elastic body  $\Omega$  embedded in a set of arbitrarily placed nodes, with none of them belonging on the global boundary  $\Gamma$  of the analyzed domain. Each node  $\mathbf{x}^{(k)}$  is the center of a circle ( $\Omega_{(k)}$ ) of radius  $r_0^{(k)}$  called support domain, as shown in Fig. 1. For an arbitrary point  $\mathbf{y}$ , the support subdomains  $\Omega_{(j)}$  of the adjacent nodes  $\mathbf{x}^{(j)}$ ,  $j = 1, \dots, n$  that contain  $\mathbf{y}$  define a non-circular subdomain:  $\hat{\Omega}_y = \Omega_{(1)} \cup \dots \cup \Omega_{(n)}$ , called domain of definition of the approximated field point. For

that node the displacement component can be approximated as [Lancaster and Salkauskas (1981)]

$$u_i(\mathbf{y}) = \mathbf{p}(\mathbf{x}) \cdot \mathbf{a}^{(i)}(\mathbf{x}) \quad (1)$$

with  $\mathbf{p}$  being a vector the  $m$  components of which form a complete basis of monomials of the spatial variables  $x_i$ , according to Pascal's triangle. The unknown coefficients of vector  $\mathbf{a}^{(i)}$  are determined by minimizing the  $L_2$ -norm:

$$J_i = \sum_{j=1}^n w(\mathbf{y}, \mathbf{x}^{(j)}) \left[ \mathbf{p}(\mathbf{x}^{(j)}) \cdot \mathbf{a}^{(i)}(\mathbf{y}) - \hat{u}_i(\mathbf{x}^{(j)}) \right]^2 \quad (2)$$

where  $\hat{u}_i(\mathbf{x}^{(j)})$  is the unknown fictitious nodal field value at node  $\mathbf{x}^{(j)}$  and  $w(\mathbf{y}, \mathbf{x}^{(j)})$  stands for the weight function. In the present paper two kinds of weight functions are used: (a) the quartic-Spline and (b) the Gaussian exponential, given below respectively

$$w(\mathbf{y}, \mathbf{x}^{(j)}) = 1 - 6l^2 + 8l^3 - 3l^4; \quad l = d/r_0^{(j)} \quad (3)$$

$$w(\mathbf{y}, \mathbf{x}^{(j)}) = 1 + \frac{\exp(-d^2/c^2) - 1}{1 - \exp(-r_0^{(j)2}/c^2)} \quad (4)$$

where  $d = \|\mathbf{y} - \mathbf{x}^{(j)}\|$  stands for the Euclidean distance of these two points and  $c$  is a parameter set equal to 0.95.

The minimization of  $J_i$  leads to the linear relation:

$$\tilde{\mathbf{A}}(\mathbf{y}, \mathbf{x}^{(j)}) \cdot \mathbf{a}^{(i)}(\mathbf{y}) = \tilde{\mathbf{B}}(\mathbf{y}, \mathbf{x}^{(j)}) \cdot \hat{\mathbf{u}}^{(i)} \quad (5)$$

where

$$\hat{\mathbf{u}}^{(i)} = \{\hat{u}_i(\mathbf{x}^{(1)}) \quad \dots \quad \hat{u}_i(\mathbf{x}^{(n)})\}^T \quad (6)$$

$$\tilde{\mathbf{A}}(\mathbf{y}, \mathbf{x}^{(j)}) = \sum_{l=1}^n w(\mathbf{y}, \mathbf{x}^{(l)}) \mathbf{p}(\mathbf{x}^{(l)}) \mathbf{p}(\mathbf{x}^{(l)})^T \quad (7)$$

$$\tilde{\mathbf{B}}(\mathbf{y}, \mathbf{x}^{(j)}) = \begin{bmatrix} w(\mathbf{y}, \mathbf{x}^{(1)}) \mathbf{p}(\mathbf{x}^{(1)}) \\ \vdots \\ w(\mathbf{y}, \mathbf{x}^{(n)}) \mathbf{p}(\mathbf{x}^{(n)}) \end{bmatrix}^T \quad (8)$$

If matrix  $\tilde{\mathbf{A}}$  is invertible and the condition  $n \geq m$  is satisfied then

$$\mathbf{a}^{(i)}(\mathbf{y}) = \tilde{\mathbf{A}}^{-1}(\mathbf{y}, \mathbf{x}^{(j)}) \cdot \tilde{\mathbf{B}}(\mathbf{y}, \mathbf{x}^{(j)}) \cdot \hat{\mathbf{u}}^{(i)} \quad (9)$$

Taking Eq. 1 and Eq. 9 someone obtains the MLS approximant of the displacement vector at the neighborhood of node  $\mathbf{y}$

$$u_i(\mathbf{y}) = \mathbf{p}(\mathbf{y}) \cdot \tilde{\mathbf{A}}^{-1}(\mathbf{y}, \mathbf{x}^{(j)}) \cdot \tilde{\mathbf{B}}(\mathbf{y}, \mathbf{x}^{(j)}) \cdot \hat{\mathbf{u}}^{(i)} \Rightarrow \mathbf{u}(\mathbf{y}) = \sum_{j=1}^n \phi(\mathbf{y}, \mathbf{x}^{(j)}) \hat{\mathbf{u}}(\mathbf{x}^{(j)}) \quad (10)$$

where  $\hat{\mathbf{u}}(\mathbf{x}^{(j)})$  is the fictitious displacement vector field at node  $\mathbf{x}^{(j)}$  and

$$\phi(\mathbf{y}, \mathbf{x}^{(j)}) = \sum_{l=1}^m p_l(\mathbf{y}) \left[ \tilde{\mathbf{A}}^{-1}(\mathbf{y}, \mathbf{x}^{(j)}) \cdot \tilde{\mathbf{B}}(\mathbf{y}, \mathbf{x}^{(j)}) \right]_{lj} \quad (11)$$

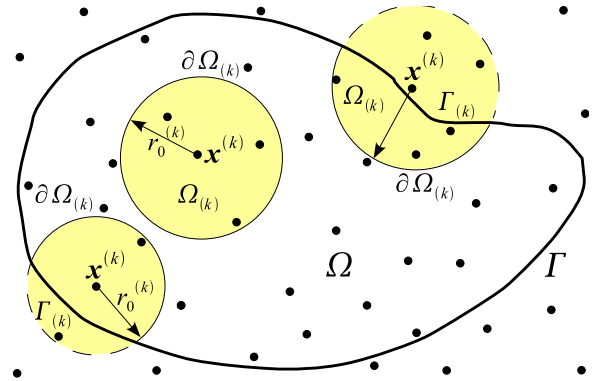


Figure 2: Support domains  $\Omega_{(k)}$  of internal and boundary nodes, and intersections with the bounding surface  $\Gamma$

### 3 LBIE formulation in Elastostatics

Consider a two-dimensional (2-D) linear elastic domain of volume  $\Omega$  surrounded by boundary  $\Gamma$  (see Fig. 2). The displacement field  $\mathbf{u}$  at any arbitrary point  $\mathbf{x}^{(k)}$  satisfies the Navier-Cauchy

equation of equilibrium [Timoshenko and Goodier (1970)]

$$\mu \nabla_{\mathbf{x}} \cdot \nabla_{\mathbf{x}} \mathbf{u}(\mathbf{x}^{(k)}) + (\lambda + \mu) \nabla_{\mathbf{x}} \nabla_{\mathbf{x}} \cdot \mathbf{u}(\mathbf{x}^{(k)}) = \mathbf{0} \quad (12)$$

where body forces are neglected,  $\lambda$  and  $\mu$  are the Lamé constants and  $\nabla_{\mathbf{x}}$  is the gradient operator with respect to vector  $\mathbf{x}$ . The Boundary Conditions (BCs) are assumed to be

$$\begin{aligned} \mathbf{u}(\mathbf{x}) &= \bar{\mathbf{u}}, \mathbf{x} \in \Gamma_u \\ \mathbf{t}(\mathbf{x}) &= \bar{\mathbf{t}}, \mathbf{x} \in \Gamma_t \end{aligned} \quad (13)$$

with  $\bar{\mathbf{u}}$ ,  $\bar{\mathbf{t}}$  representing prescribed displacement and traction vectors, respectively, on the global boundary  $\Gamma = \Gamma_u \cup \Gamma_t$ .

The integral representation of the above described problem is [Brebbia and Dominguez (1989)]

$$\begin{aligned} a \mathbf{u}(\mathbf{x}^{(k)}) + \int_{\Gamma} \tilde{\mathbf{t}}^*(\mathbf{x}^{(k)}, \mathbf{y}) \cdot \mathbf{u}(\mathbf{y}) dS_{\mathbf{y}} \\ = \int_{\Gamma} \tilde{\mathbf{u}}^*(\mathbf{x}^{(k)}, \mathbf{y}) \cdot \mathbf{t}(\mathbf{y}) dS_{\mathbf{y}} \end{aligned} \quad (14)$$

where  $a$  takes the values 1, 0 for internal and external points, respectively, while  $\tilde{\mathbf{u}}^*$ ,  $\tilde{\mathbf{t}}^*$  stand for the 2-D elastostatic fundamental displacement and traction second-order tensors [Banerjee (1994); Brebbia and Dominguez (1989); Polyzos, Tsinopoulos, and Beskos (1998)], respectively.

Applying the gradient operator on Eq. 14 and utilizing Hooke's law, the corresponding hypersingular boundary integral equation of stresses is derived, i.e.

$$\begin{aligned} a \tilde{\sigma}(\mathbf{x}^{(k)}) + \int_{\Gamma} \tilde{\tilde{\mathbf{t}}}^*(\mathbf{x}^{(k)}, \mathbf{y}) \cdot \mathbf{u}(\mathbf{y}) dS_{\mathbf{y}} \\ = \int_{\Gamma} \tilde{\tilde{\mathbf{u}}}^*(\mathbf{x}^{(k)}, \mathbf{y}) \cdot \mathbf{t}(\mathbf{y}) dS_{\mathbf{y}} \end{aligned} \quad (15)$$

where  $\tilde{\sigma}$  is the stress tensor and the third-order tensors  $\tilde{\tilde{\mathbf{u}}}^*$ ,  $\tilde{\tilde{\mathbf{t}}}^*$  are kernels given in the book of Banerjee (1994), while for both compressible and

incompressible elastic materials are given in reference [Polyzos, Tsinopoulos, and Beskos (1998)].

Exploiting the symmetry of tensor  $\tilde{\sigma}$ , the surface traction vector  $\mathbf{t}$  can be written in the form

$$\mathbf{t}(\mathbf{y}) = \begin{bmatrix} \hat{n}_1 & 0 & \hat{n}_2 \\ 0 & \hat{n}_2 & \hat{n}_1 \end{bmatrix} \cdot \begin{Bmatrix} \sigma_{11} \\ \sigma_{22} \\ \sigma_{12} \end{Bmatrix} = \tilde{\mathbf{N}}(\mathbf{y}) \cdot \boldsymbol{\tau}(\mathbf{y}) \quad (16)$$

where  $\hat{n}_i$  are the components of the outward unit normal vector to surface  $\Gamma$  and  $\sigma_{11}$ ,  $\sigma_{22}$  and  $\sigma_{12}$  the independent components of stress tensor  $\tilde{\sigma}$ .

Substituting Eq. 16 in Eq. 14 and 15 one obtains

$$\begin{aligned} a \mathbf{u}(\mathbf{x}^{(k)}) + \int_{\Gamma} \tilde{\mathbf{t}}^*(\mathbf{x}^{(k)}, \mathbf{y}) \cdot \mathbf{u}(\mathbf{y}) dS_{\mathbf{y}} \\ = \int_{\Gamma} \tilde{\mathbf{u}}^*(\mathbf{x}^{(k)}, \mathbf{y}) \cdot \tilde{\mathbf{N}}(\mathbf{y}) \cdot \boldsymbol{\tau}(\mathbf{y}) dS_{\mathbf{y}} \end{aligned} \quad (17)$$

$$\begin{aligned} a \boldsymbol{\tau}(\mathbf{x}^{(k)}) + \int_{\Gamma} \tilde{\mathbf{T}}^*(\mathbf{x}^{(k)}, \mathbf{y}) \cdot \mathbf{u}(\mathbf{y}) dS_{\mathbf{y}} \\ = \int_{\Gamma} \tilde{\mathbf{U}}^*(\mathbf{x}^{(k)}, \mathbf{y}) \cdot \tilde{\mathbf{N}}(\mathbf{y}) \cdot \boldsymbol{\tau}(\mathbf{y}) dS_{\mathbf{y}} \end{aligned} \quad (18)$$

where the kernels  $\tilde{\mathbf{U}}^*$ ,  $\tilde{\mathbf{T}}^*$  are taken after rearrangement of  $\tilde{\mathbf{u}}^*$ ,  $\tilde{\mathbf{t}}^*$ , respectively, since according to Eq. 16,  $\boldsymbol{\tau}$  is a three-dimensional vector.

It is well-known that the above set of integral equations become singular only when the field point  $\mathbf{y}$  coincides with the source point  $\mathbf{x}^{(k)}$ . Thus, Eqs. 17 and 18 can be also written in the form

$$\begin{aligned} a \mathbf{u}(\mathbf{x}^{(k)}) + \int_{\partial\Omega_{(k)} \cup \Gamma_{(k)}} \tilde{\mathbf{t}}^*(\mathbf{x}^{(k)}, \mathbf{y}) \cdot \mathbf{u}(\mathbf{y}) dS_{\mathbf{y}} \\ = \int_{\partial\Omega_{(k)} \cup \Gamma_{(k)}} \tilde{\mathbf{u}}^*(\mathbf{x}^{(k)}, \mathbf{y}) \cdot \tilde{\mathbf{N}}(\mathbf{y}) \cdot \boldsymbol{\tau}(\mathbf{y}) dS_{\mathbf{y}} \end{aligned} \quad (19)$$

$$\begin{aligned} a \boldsymbol{\tau}(\mathbf{x}^{(k)}) + \int_{\partial\Omega_{(k)} \cup \Gamma_{(k)}} \tilde{\mathbf{T}}^*(\mathbf{x}^{(k)}, \mathbf{y}) \cdot \mathbf{u}(\mathbf{y}) dS_{\mathbf{y}} \\ = \int_{\partial\Omega_{(k)} \cup \Gamma_{(k)}} \tilde{\mathbf{U}}^*(\mathbf{x}^{(k)}, \mathbf{y}) \cdot \tilde{\mathbf{N}}(\mathbf{y}) \cdot \boldsymbol{\tau}(\mathbf{y}) dS_{\mathbf{y}} \end{aligned} \quad (20)$$

where  $\partial\Omega_{(k)}$ ,  $\Gamma_{(k)}$  are illustrated in Fig. 2.

In case when the support domain  $\Omega_{(k)}$  does not intersect with the global boundary  $\Gamma$  then the boundary integrals on  $\Gamma_{(k)}$  vanish from both Eq. 19 and 20.

Splitting the boundary integrals on  $\Gamma_{(k)}$  according to the prescribed BCs then one obtains

$$\begin{aligned} & a \mathbf{u}(\mathbf{x}^{(k)}) + \int_{\partial\Omega_{(k)} \cup \Gamma_{(k)t}} \tilde{\mathbf{t}}^*(\mathbf{x}^{(k)}, \mathbf{y}) \cdot \mathbf{u}(\mathbf{y}) dS_{\mathbf{y}} \\ & - \int_{\partial\Omega_{(k)} \cup \Gamma_{(k)u}} \tilde{\mathbf{u}}^*(\mathbf{x}^{(k)}, \mathbf{y}) \cdot \tilde{\mathbf{N}}(\mathbf{y}) \cdot \boldsymbol{\tau}(\mathbf{y}) dS_{\mathbf{y}} \\ & = \int_{\Gamma_{(k)t}} \tilde{\mathbf{u}}^*(\mathbf{x}^{(k)}, \mathbf{y}) \cdot \bar{\mathbf{t}}(\mathbf{y}) dS_{\mathbf{y}} \\ & - \int_{\Gamma_{(k)u}} \tilde{\mathbf{t}}^*(\mathbf{x}^{(k)}, \mathbf{y}) \cdot \bar{\mathbf{u}}(\mathbf{y}) dS_{\mathbf{y}} \end{aligned} \quad (21)$$

$$\begin{aligned} & a \boldsymbol{\tau}(\mathbf{x}^{(k)}) + \int_{\partial\Omega_{(k)} \cup \Gamma_{(k)t}} \tilde{\mathbf{T}}^*(\mathbf{x}^{(k)}, \mathbf{y}) \cdot \mathbf{u}(\mathbf{y}) dS_{\mathbf{y}} \\ & - \int_{\partial\Omega_{(k)} \cup \Gamma_{(k)u}} \tilde{\mathbf{U}}^*(\mathbf{x}^{(k)}, \mathbf{y}) \cdot \tilde{\mathbf{N}}(\mathbf{y}) \cdot \boldsymbol{\tau}(\mathbf{y}) dS_{\mathbf{y}} \\ & = \int_{\Gamma_{(k)t}} \tilde{\mathbf{U}}^*(\mathbf{x}^{(k)}, \mathbf{y}) \cdot \bar{\mathbf{t}}(\mathbf{y}) dS_{\mathbf{y}} \\ & - \int_{\Gamma_{(k)u}} \tilde{\mathbf{T}}^*(\mathbf{x}^{(k)}, \mathbf{y}) \cdot \bar{\mathbf{u}}(\mathbf{y}) dS_{\mathbf{y}} \end{aligned} \quad (22)$$

whereas  $\Gamma_{(k)} = \Gamma_{(k)u} \cup \Gamma_{(k)t}$ .

Considering for both  $\mathbf{u}$  and  $\boldsymbol{\tau}$  the MLS approximation scheme presented in section 2, Eq. 21 and 22 read

$$\begin{aligned} & a \sum_{j=1}^n \phi(\mathbf{x}^{(k)}, \mathbf{x}^{(j)}) \hat{\mathbf{u}}(\mathbf{x}^{(j)}) \\ & + \sum_{j=1}^n \int_{\partial\Omega_{(k)} \cup \Gamma_{(k)t}} \tilde{\mathbf{t}}^*(\mathbf{x}^{(k)}, \mathbf{y}) \phi(\mathbf{y}, \mathbf{x}^{(j)}) dS_{\mathbf{y}} \\ & \cdot \hat{\mathbf{u}}(\mathbf{x}^{(j)}) \\ & - \sum_{j=1}^n \int_{\partial\Omega_{(k)} \cup \Gamma_{(k)u}} \tilde{\mathbf{u}}^*(\mathbf{x}^{(k)}, \mathbf{y}) \cdot \tilde{\mathbf{N}}(\mathbf{y}) \phi(\mathbf{y}, \mathbf{x}^{(j)}) dS_{\mathbf{y}} \\ & \cdot \hat{\boldsymbol{\tau}}(\mathbf{x}^{(j)}) \\ & = \int_{\Gamma_{(k)t}} \tilde{\mathbf{u}}^*(\mathbf{x}^{(k)}, \mathbf{y}) \cdot \bar{\mathbf{t}}(\mathbf{y}) dS_{\mathbf{y}} \\ & - \int_{\Gamma_{(k)u}} \tilde{\mathbf{t}}^*(\mathbf{x}^{(k)}, \mathbf{y}) \cdot \bar{\mathbf{u}}(\mathbf{y}) dS_{\mathbf{y}} \end{aligned} \quad (23)$$

$$\begin{aligned} & a \sum_{j=1}^n \phi(\mathbf{x}^{(k)}, \mathbf{x}^{(j)}) \hat{\boldsymbol{\tau}}(\mathbf{x}^{(j)}) \\ & + \sum_{j=1}^n \int_{\partial\Omega_{(k)} \cup \Gamma_{(k)t}} \tilde{\mathbf{T}}^*(\mathbf{x}^{(k)}, \mathbf{y}) \phi(\mathbf{y}, \mathbf{x}^{(j)}) dS_{\mathbf{y}} \\ & \cdot \hat{\mathbf{u}}(\mathbf{x}^{(j)}) \\ & - \sum_{j=1}^n \int_{\partial\Omega_{(k)} \cup \Gamma_{(k)u}} \tilde{\mathbf{U}}^*(\mathbf{x}^{(k)}, \mathbf{y}) \cdot \tilde{\mathbf{N}}(\mathbf{y}) \phi(\mathbf{y}, \mathbf{x}^{(j)}) dS_{\mathbf{y}} \\ & \cdot \hat{\boldsymbol{\tau}}(\mathbf{x}^{(j)}) \\ & = \int_{\Gamma_{(k)t}} \tilde{\mathbf{U}}^*(\mathbf{x}^{(k)}, \mathbf{y}) \cdot \bar{\mathbf{t}}(\mathbf{y}) dS_{\mathbf{y}} \\ & - \int_{\Gamma_{(k)u}} \tilde{\mathbf{T}}^*(\mathbf{x}^{(k)}, \mathbf{y}) \cdot \bar{\mathbf{u}}(\mathbf{y}) dS_{\mathbf{y}} \end{aligned} \quad (24)$$

For the numerical evaluation of all boundary integrals involved in the above equations one can consult the thorough papers [Atluri, Kim, and Cho (1999); Sladek, Sladek, and Keer (2000a); Sellountos and Polyzos (2003)].

As seen in Eq. 23 and 24, the only unknown quantities are the fictitious nodal displacements and stresses. Considering a distribution of  $N$  nodes (Fig. 2) and collocating both Eq. 23 and 24 one can conclude to the final linear system of equations

$$\tilde{\mathbf{A}} \cdot \mathbf{v} = \mathbf{b} \quad (25)$$

where the  $5N \times 5N$  sparse matrix  $\tilde{\mathbf{A}}$  contains all the boundary integrals and free-terms of the left-hand side of Eqs. 23 and 24, the right-hand-side vector  $\mathbf{b}$  contains the boundary integrals on  $\Gamma$  with prescribed BCs and vector  $\mathbf{v}$  contains the unknown fictitious nodal displacements and stresses.

After solving the linear system of Eq. 25 and obtaining the fictitious nodal displacements and stresses then one can make use of the approximation Eq. 10, so as to retrieve the true nodal values of the analyzed elastic body.

#### 4 Numerical Examples

This section presents some numerical examples, which demonstrate the achieved accuracy of the proposed here MLPG(LBIE) methodology.

The accuracy of the obtained numerical results is validated by means of the relative error  $L_2$  norm

$$err_v = \log_{10} \sqrt{\frac{\sum_{i=1}^N \|\mathbf{v}_{analytical}^{(i)} - \mathbf{v}_{numerical}^{(i)}\|^2}{\sum_{i=1}^N \|\mathbf{v}_{analytical}^{(i)}\|^2}} \quad (26)$$

#### 4.1 Dirichlet patch test

Consider the standard linear patch test [Belytschko, Lu, and Gu (1994)] in a square  $4 \times 4$  domain having  $E = 1$  Young modulus of elasticity and  $\nu = 0.25$  Poisson's ratio. This is a Dirichlet boundary value problem having the solution

$$\begin{aligned} u_1 &= a_0 + a_1 x_1 + a_2 x_2 \\ u_2 &= b_0 + b_1 x_1 + b_2 x_2 \end{aligned} \quad (27)$$

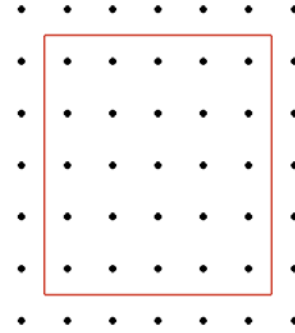
where  $a_i$  and  $b_i$  are arbitrarily-chosen constants. The displacements are prescribed on all four sides according to Eq. 27, while the stress field is constant in the patch.

Since the exact solution of the displacement field is linear, a first order polynomial basis for the MLS is adequate to represent the approximated field quantities. The quartic-Spline weight function of Eq. 3 is used for the MLS scheme. The square domain of Fig. 3(a) is discretized with a uniform distribution of 49 nodes. As observed in the same figure, no boundary points are used in analyzing the problem, thus, no singularities on the integrated kernels are met. Consequently, the classical Gauss-Legendre integration scheme is utilized with 8 quadrature points.

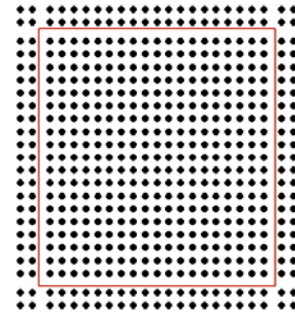
From the derived numerical results obtained for various normalized support domain radii  $r_0/d$  ( $d$  is the distance of two consecutive nodes), as presented in Fig. 4, it can be stated that the MLPG(LBIE) method solves this problem with high accuracy.

#### 4.2 Higher order patch tests

Two high-order patch tests [Belytschko, Lu, and Gu (1994); Taylor, Beresford, and Wilson (1976)] are further studied having mixed-type BCs on all



(a)



(b)

Figure 3: Uniform distribution of (a) 49 and (b) 529 nodes in the square domain

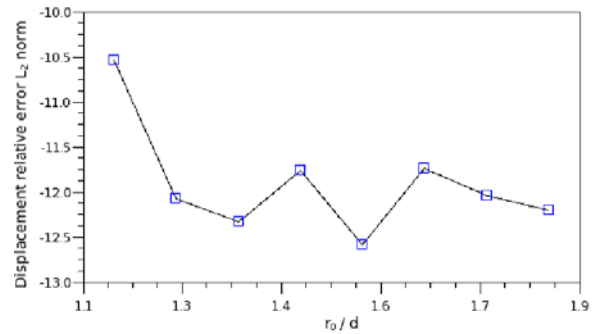


Figure 4: Dirichlet patch test: displacement relative error  $L_2$  norm for various support domains (49-node mesh)

boundary sides, as it is explained in Fig. 5. On the first case (linear patch test) the horizontal force load applied on the right side of the rectangle is considered uniform ( $\bar{t}_1 = p$ ), whereas the analytical solutions to this problem are given below

$$\begin{aligned} u_1 &= p x_1 / \bar{E} \\ u_2 &= -p x_2 / \bar{E} \end{aligned} \quad (28)$$

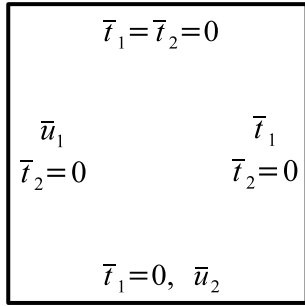


Figure 5: Rectangular domain of the higher order patch test with its prescribed BCs

On the second case (quadratic patch test) the traction load is linearly varied ( $\bar{t}_1 = px_2$ ), while the analytical solutions of the displacement field are the following

$$\begin{aligned} u_1 &= px_1x_2/\bar{E} \\ u_2 &= -p(x_1^2 + \bar{\nu}x_2^2)/(2\bar{E}) \end{aligned} \quad (29)$$

where  $\bar{E} = E$ ,  $\bar{\nu} = \nu$  for plane-stress and  $\bar{E} = E/(1 - \nu^2)$ ,  $\bar{\nu} = \nu/(1 - \nu)$  for plane-strain. The material properties are kept the same just as in subsection 4.1.

For the case of Eqs. 28 the relative error  $L_2$  norm of displacements is shown in Fig. 6. The nodal points are the same to those used in the linear patch test of 4.1. As it is seen, the obtained results show a rather stable behaviour and excellent accuracy, even though a non-dense mesh is utilized and a linear basis on the MLS approximation is employed.

In the case of the quadratic domain 2nd and 3rd order polynomial basis are utilized in the MLS approximation to represent the solution. The domain is covered by a 49-node and a 529-node uniform mesh, as demonstrated in Fig. 3. The corresponding  $L_2$  norms are presented in Fig. 7 and 8, for both MLS polynomial bases. As observed, the higher polynomial basis in the MLS chosen the more stable results are acquired. Also denser distribution of points delivers more accurate results.

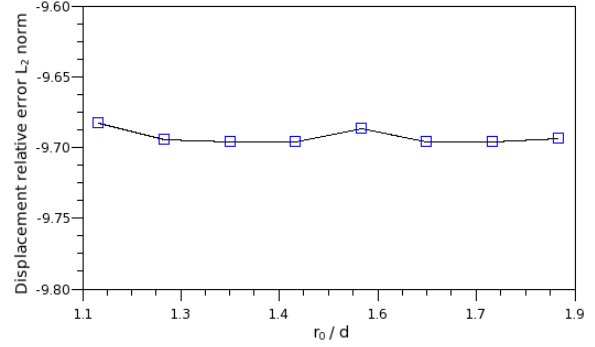


Figure 6: Linear high-order patch test: displacement relative error  $L_2$  norm for various support domains for MLS with linear basis (49-node mesh)

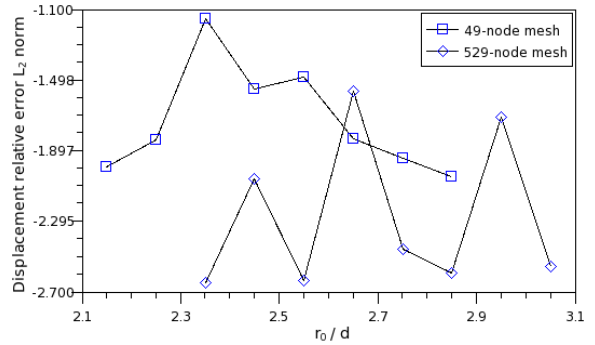


Figure 7: Quadratic high-order patch test: displacement relative error  $L_2$  norm for various support domains for MLS with quadratic basis

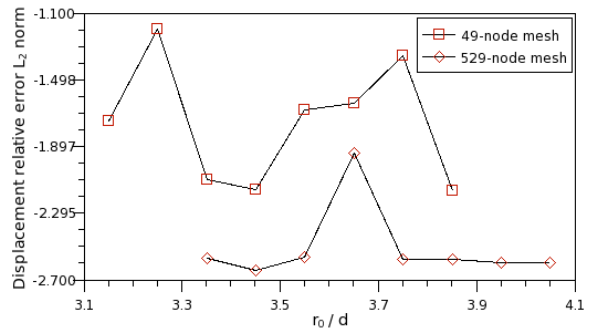


Figure 8: Quadratic high-order patch test: displacement relative error  $L_2$  norm for various support domains for MLS with cubic basis

### 4.3 Cantilever beam

The exact solution of the displacement and stress field for the cantilever beam, subjected to a shear

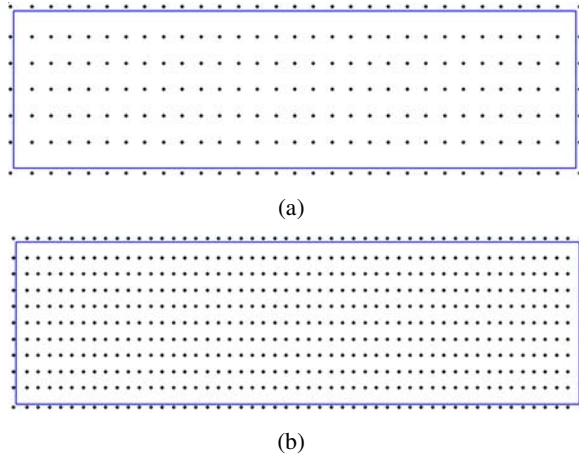


Figure 9: Uniform distribution of (a) 217 and (b) 561 nodes for a cantilever beam

load applied on the right free-end, is given in the book of Timoshenko and Goodier (1970).

$$u_1 = -\frac{p}{6EI} (x_2 - D/2) [x_1 (6L - 3x_1) + (2 + \bar{\nu}) x_2 (x_2 - D)] \quad (30)$$

$$u_2 = \frac{p}{6EI} \left[ 3\bar{\nu}(L - x_1) (x_2 - D/2)^2 + (4 + 5\bar{\nu}) x_1 D^2 / 4 + (3L - x_1) x_1^2 \right] \quad (31)$$

$$\sigma_{11} = -\frac{p}{I} (L - x_1) (x_2 - D/2) \quad (32)$$

$$\sigma_{22} = 0 \quad (33)$$

$$\sigma_{12} = -\frac{p}{2I} x_2 (x_2 - D) \quad (34)$$

where the moment of inertia:  $I = D^3/12$ , for a rectangular cross-section of thickness  $D = 1$ , length  $L = 5$  and unit shear load  $p = 1$ . The constants  $\bar{E}$  and  $\bar{\nu}$  are the same with those of subsection 4.2.

Figures 10 and 11 depict displacements and stresses relative error  $L_2$  norms, respectively, for both meshes. The main conclusion here is that the solution is drastically affected by the size of the considered support domain, while both stresses and displacements are obtained with almost the same accuracy.

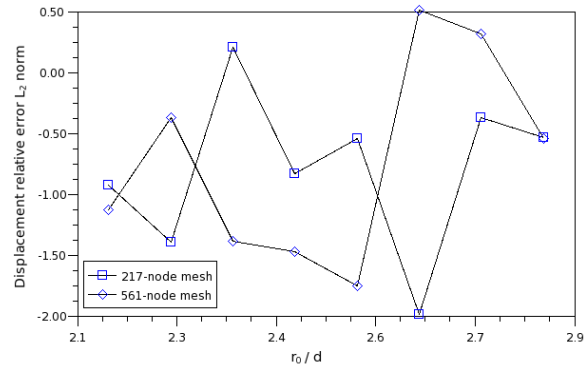


Figure 10: Cantilever beam problem: displacement relative error  $L_2$  norm for various support domains for MLS with quadratic basis

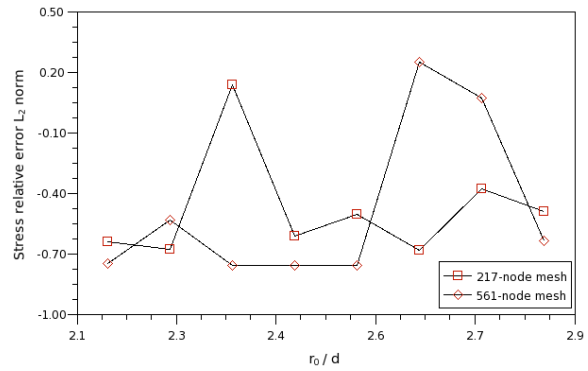


Figure 11: Cantilever beam problem: stress relative error  $L_2$  norm for various support domains for MLS with quadratic basis

#### 4.4 Lamé problem

The Lamé problem consists of a hollow cylinder subjected to a uniform internal pressure load ( $p = 1$ ) under plane-strain conditions. The cylinder has internal radius  $a = 0.5$  and external radius  $b = 1$ , while the material properties are  $E = 1.0$  and  $\nu = 0.25$ . The exact solutions of the displacement and the stress field, given in polar coordinates  $(r, \theta)$  with the origin at the center of the cylinder, are the ones given below [Timoshenko and Goodier (1970)]

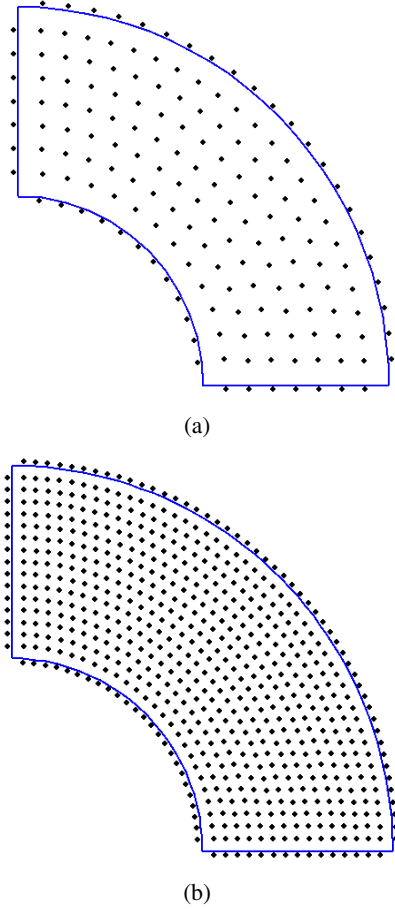


Figure 12: Uniform distribution of (a) 118 and (b) 536 nodes in the quarter cylinder

$$u_1 = \frac{pa^2}{b^2 - a^2} \frac{1 + \bar{\nu}}{E} \left[ (1 - 2\bar{\nu})r + \frac{b^2}{r} \right] \quad (35)$$

$$u_2 = 0 \quad (36)$$

$$\sigma_{11} = \frac{pa^2}{b^2 - a^2} \left( 1 - \frac{b^2}{r^2} \right) \quad (37)$$

$$\sigma_{22} = \frac{pa^2}{b^2 - a^2} \left( 1 + \frac{b^2}{r^2} \right) \quad (38)$$

$$\sigma_{12} = 0 \quad (39)$$

Due to symmetry, only the upper right quadrant of the cylinder is analyzed, as shown in Fig. 12, with 118 and 536 nodes distributed internally and externally to the domain of interest. Symmetry conditions are imposed on the bottom ( $\bar{u}_2 = 0$ ) and left edge ( $\bar{u}_1 = 0$ ) of the quadrant, while the outer surface is traction-free.

In this numerical example, the Gaussian weight function of Eq. 4 is used in the MLS approximation method. For both displacement and stress fields quadratic and cubic polynomial bases are assumed.

In Fig. 13 and 15 the displacement relative  $L_2$  error norms are shown for both node distributions in quadratic and cubic basis, respectively. The same is presented for stresses in Fig. 14 and 16.

Again, one can say that the radii of the considered support domains affect drastically the accuracy of the obtained results. The cubic basis used in MLS scheme seems to deliver more accurate and more stable results than the quadratic one.

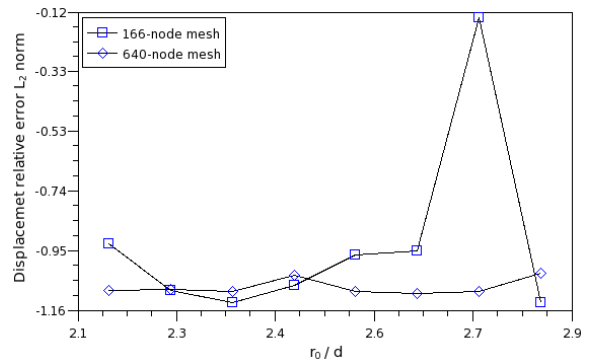


Figure 13: Lamé problem: displacement relative error  $L_2$  norm for various support domains for MLS with quadratic basis

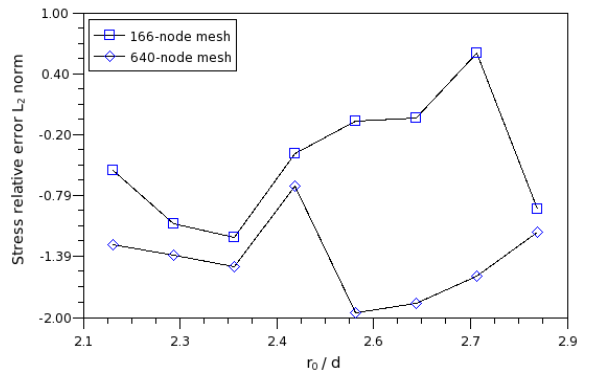


Figure 14: Lamé problem: stress relative error  $L_2$  norm for various support domains for MLS with quadratic basis

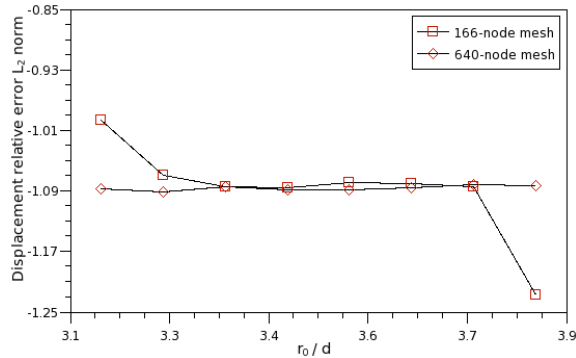


Figure 15: Lamé problem: displacement relative error  $L_2$  norm for various support domains for MLS with cubic basis

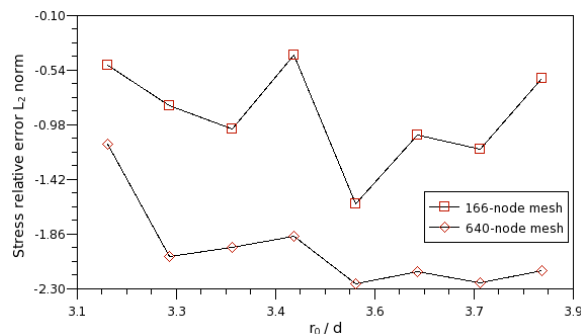


Figure 16: Lamé problem: stress relative error  $L_2$  norm for various support domains for MLS with cubic basis

## 5 Conclusions

A new MLPG(LBIE) method capable to solve 2D elastostatic problems has been presented. The new elements and the main conclusions of this work can be summarized as follows

- (i) The method considers displacements and stresses as independent variables at any nodal point of the analyzed domain. This is accomplished with the aid of the corresponding local integral representations valid for internal and external nodes. Of course, the use of three more degrees of freedom makes the proposed MLPG(LBIE) method more time-consuming as it is compared to other MLPG(LBIE) formulations. However, this disadvantage is compensated by the facts that (a) stresses are evaluated with

the same accuracy as displacements and (b) MLPG(LBIE) becomes more accurate when no derivatives of MLS approximation functions are involved in its formulation [Vavourakis, Sellountos, and Polyzos (2006)].

- (ii) Since no points on the global boundary are placed, all the integrals involved in the present MPG(LBIE) formulation are regular.
- (iii) The radii of the considered support domains affect the accuracy of the obtained results
- (iv) Cubic polynomial basis in the MLS scheme provides more accurate and more stable results than the quadratic one.

Finally, the accuracy achieved by the proposed MLPG(LBIE) method is demonstrated with three representative numerical examples.

**Acknowledgement:** We thank the European Social Fund (ESF), Operational Program for Educational and Vocational Training II (EPEAEK II), and particularly the Program PYTHAGORAS II, for funding the above work.

## References

- Atluri, S. N.** (2004): *The Meshless Method (MLPG) for Domain & BIE Discretization*. Tech. Science Press.
- Atluri, S. N.; Han, Z. D.; Shen, S.** (2003): Meshless local Petrov-Galerkin (MLPG) approaches for solving the weakly-singular traction and displacement boundary integral equations. *CMES: Computer Modeling in Engineering & Sciences*, vol. 4, pp. 507–517.
- Atluri, S. N.; Kim, H.-G.; Cho, J. Y.** (1999): A critical assessment of the truly Meshless Local Petrov-Galerkin (MLPG) and Local Boundary Integral Equation (LBIE) methods. *Computational Mechanics*, vol. 24, pp. 348–372.
- Atluri, S. N.; Shen, S.** (2002): The meshless local Petrov-Galerkin (MLPG) method: A simple & less-costly alternative to the finite and boundary

element method. *CMES: Computer Modeling in Engineering & Sciences*, vol. 3, pp. 11–52.

**Atluri, S. N.; Shen, S.** (2002): *The Meshless Local Petrov-Galerkin (MLPG) Method*. Tech. Science Press.

**Atluri, S. N.; Sladek, J.; Sladek, V.; Zhu, T.** (2000): The local boundary integral equation (LBIE) and its meshless implementation for linear elasticity. *Computational Mechanics*, vol. 25, pp. 180–198.

**Atluri, S. N.; Zhu, T.** (1998): A new meshless local Petrov-Galerkin (MLPG) approach in computation mechanics. *Computational Mechanics*, vol. 22, pp. 117–127.

**Banerjee, P. K.** (1994): *The Boundary Element Methods in Engineering*. McGraw-Hill.

**Belytschko, T.; Lu, Y. Y.; Gu, L.** (1994): Element-free Galerkin methods. *International Journal for Numerical Methods in Engineering*, vol. 37, pp. 229–256.

**Bodin, A.; Ma, J.; Xin, X. J.; Krishnaswami, P.** (2006): A meshless integral method based on regularized boundary integral equation. *Computer Methods in Applied Mechanics and Engineering*, vol. 195, pp. 6258–6286.

**Brebbia, C. A.; Dominguez, J.** (1989): *Boundary Elements: An introductory course*. Computational Mechanics Publications, Southampton.

**Han, Z. D.; Atluri, S. N.** (2004): Meshless local Petrov-Galerkin (MLPG) approaches for solving 3D Problems in elasto-statics. *CMES: Computer Modelling in Engineering & Sciences*, vol. 6, pp. 169–188.

**Lancaster, P.; Salkauskas, K.** (1981): Surfaces generated by moving least squares methods. *Mathematics of Computations*, vol. 37, pp. 141–158.

**Liu, G. R.** (2003): *Mesh Free Methods*. CRC Press.

**Polyzos, D.; Tsinopoulos, S. V.; Beskos, D. E.** (1998): Static and dynamic boundary element

analysis in incompressible linear elasticity. *European Journal of Mechanics, A/Solids*, vol. 17, pp. 515–536.

**Sellountos, E. J.; Polyzos, D.** (2003): A MLPG (LBIE) method for solving frequency domain elastic problems. *CMES: Computer Modelling in Engineering & Sciences*, vol. 4, pp. 619–636.

**Sellountos, E. J.; Polyzos, D.** (2005a): A MLPG (LBIE) approach in combination with BEM. *Computer Methods in Applied Mechanics and Engineering*, vol. 194, pp. 859–875.

**Sellountos, E. J.; Polyzos, D.** (2005b): A meshless local boundary integral equation method for solving transient elastodynamic problems. *Computational Mechanics*, vol. 35, pp. 265–276.

**Sellountos, E. J.; Vavourakis, V.; Polyzos, D.** (2005): A new Singular/Hypersingular MLPG (LBIE) method for 2D elastostatics. *CMES: Computer Modeling in Engineering & Sciences*, vol. 7, no. 1, pp. 35–48.

**Sladek, J.; Sladek, V.; Atluri, S. N.** (2000b): Local boundary integral equation (LBIE) method for solving problems of elasticity with non-homogeneous material properties. *Computational Mechanics*, vol. 24, pp. 456–462.

**Sladek, J.; Sladek, V.; Atluri, S. N.** (2002): Application of the local boundary integral equation method to boundary value problems. *International Journal of Applied Mechanics*, vol. 38, pp. 1025–1043.

**Sladek, J.; Sladek, V.; Keer, R. V.** (2000a): Numerical integration of singularities of local boundary integral equations. *Computational Mechanics*, vol. 25, pp. 394–403.

**Taylor, R. L.; Beresford, P. J.; Wilson, E. L.** (1976): A non-conforming element for stress analysis. *International Journal for Numerical Methods in Engineering*, vol. 10, pp. 1211–1219.

**Timoshenko, S. P.; Goodier, J. N.** (1970): *Theory of Elasticity*. McGraw-Hill.

**Vavourakis, V.; Sellountos, E. J.; Polyzos, D.** (2006): A comparison study on different MLPG(LBIE) formulations. *CMES: Computer Modelling in Engineering & Sciences*, vol. 13, pp. 171–184.

**Zhu, T.; Zhang, J. D.; Atluri, S. N.** (1998): A local boundary integral equation (LBIE) method in computational mechanics and a meshless discretization approach. *Computational Mechanics*, vol. 21, pp. 223–235.